Spatially Consistent Street-by-Street Path Loss Model for 28-GHz Channels in Micro Cell Urban Environments

Aki Karttunen, *Member, IEEE*, Andreas F. Molisch, *Fellow, IEEE*, Sooyoung Hur, *Member, IEEE*, Jeongho Park, and Charlie Jianzhong Zhang, *Fellow, IEEE*

***Abstract*— This paper considers a fundamental issue of path loss (PL) modeling in urban micro cell (UMi) environments, namely the spatial consistency of the model as the mobile station moves along a trajectory through street canyons. This paper is motivated by the observed non-stationarity of the PL. We show that the traditional model of power law PL plus log-normally distributed variations can provide misleading results that can have serious implications for system simulations. Rather, the PL parameters have to be modeled as random variables that change from street to street and also as a function of the street orientation. Variations of the PL, taken over the ensemble of the whole cell (or multiple cells), thus consist of the compound effect of these PL parameter variations together with the traditional shadowing variations along the trajectory of movement. Ray-tracing results demonstrate that ignoring this effect can lead to a severe overestimation of the local standard deviation in a given area. Then, a spatially consistent stochastic street-by-street PL model is established, and a parameterization for 28-GHz UMi cells is given. The model correctly describes the PL as a function of the street orientation as well as the large variance observed for all the PL model parameters.**

***Index Terms*— 5G, channel model, millimeter-wave, short-range communications, path loss, spatial consistency.**

I. Introduction

FREQUENCY bands above 6-GHz, including millimeter-wave (mm-wave) bands, will play an important role in next-generation wireless communications (5G) systems, mostly due to the large amount of available bandwidth in this frequency range [2], [3]. Millimeter-wave communication systems first received attention in the 1990s. They did not gain momentum at that time, both because of the high cost of chip manufacturing for this frequency range, and the availability of cheaper alternatives to increase the data rates for cellular access. However, recent years have seen the emergence of CMOS for mm-wave, enabling the low-cost mass production of chips, and a renewed urgency in finding new spectrum for high-rate communications. This has led to renewed interest in mm-wave frequency bands and systems [2]–[4]. Channel models are an essential prerequisite for the design, simulation, performance assessment, and deployment planning of all wireless communications systems [5]. For this reason, a number of organizations, e.g., [6]–[9], are currently creating 5G channel models applicable to frequency bands above 6 GHz.

The large scale attenuation a signal experiences between transmitter and receiver, averaged over small-scale fading, is called path loss (PL). It is the most fundamental aspect of a channel model as it determines the distance range over which communication can take place. Due to its importance, many standardized PL models have been developed for indoor and outdoor, e.g. [8], [10], [11]. In order to properly reflect reality, PL models should be based on measurement campaigns, such as [12]–[18], and/or calibrated ray tracing [19]–[21].

An aspect that is especially important for 5G models is *spatial consistency*, i.e., the correct modeling of the joint channel parameters (especially PL) at different locations, or equivalently the behavior as the mobile station (MS) moves along a track. More specifically, in this paper, we examine the spatial consistency of PL as the MS moves along a trajectory through street canyons in urban micro cell (UMi) environments; UMi is one of the most important deployment scenarios for mm-wave systems, since they are well suited for short-distance communication with high density of users. Traditional channel models, such as the ones used in 3GPP [8], [10], mainly aimed to correctly describe the probability density function of the PL as a function of the link distance. System simulations were done by placing MSs at various distances, and for each placement drawing the PL according to the given probability density function. For such "dropping" simulations, existing PL models work well. However, modern systems, and in particular mm-wave systems, need to implement suitable multi-RAT (radio access technology) switching and other functions that depend on the large scale evolution of the PL as the MS moves along its route. As we will show in this paper, the "shadowing variance" obtained from traditional channel

Manuscript received June 1, 2016; revised October 21, 2016, February 26, 2017, and July 8, 2017; accepted August 25, 2017. Date of publication September 12, 2017; date of current version November 9, 2017. This work was supported by the National Science Foundation. The work of A. Karttunen was supported in part by the Walter Ahlström Foundation and in part by the Tutkijat Maailmalle Program. Initial results related to this work have been presented at the 10th European Conference on Antennas and Propagation, Davos, Switzerland, April 2016 [1]. The associate editor coordinating the review of this paper and approving it for publication was C. R. Anderson. *(Corresponding author: Aki Karttunen.)*

A. Karttunen was with the Department of Electrical Engineering, University of Southern California, Los Angeles, CA 90089-2560 USA. He is now with the Aalto University School of Electrical Engineering, 02015 Espoo, Finland (e-mail: aki.karttunen@aalto.fi).

A. F. Molisch is with the Department of Electrical Engineering, University of Southern California, Los Angeles, CA 90089-2560 USA (e-mail: molisch@usc.edu).

S. Hur, J. Park, and C. J. Zhang are with Samsung, Suwon 443-742, South Korea (e-mail: sooyoung.hur@samsung.com; jeongho.jh.park@samsung.com; jianzhong.z@samsung.com).

Color versions of one or more of the figures in this paper are available online at http://ieeexplore.ieee.org.

Digital Object Identifier 10.1109/TWC.2017.2749570

modeling can significantly overestimate the signal variations along such a route, and thus provide a misleading picture of the system performance. The reason for this error lies in the fact that traditional methods commingle variations of the PL along a route with variations between different routes either within the same cell or between different cells. Equivalently, we can say that the PL is non-stationary, i.e., the PL depends on the absolute location of the base station (BS) and MS, rather than only on the distance between them.

Several papers have considered various aspects of PL stationarity in the microwave regime. In [22], it is shown that PL parameters in different cells (in the same type of environment) can be different, and should be modeled as random variables following a truncated Gaussian distribution; furthermore, even the shadowing variance should be modeled as a random variable. The work was later extended by [23] to indoor scenarios, again showing variations of the PL coefficient and shadowing variance from building to building. Recent work by one of the authors [24] has shown that in an urban environment we should expect variations not only from cell to cell but also from street to street. In [25] and [26], different PL slopes on different streets are observed in urban environments. In [27], it is found that it could be beneficial to add an intersection dependent loss parameter to a 5.9 GHz NLOS path loss model for intersections. Non-stationarity in PL parameters is observed in measurement results with multiple radio frequencies ranging from 0.8 to 60 GHz in urban street canyons in [16]. The frequency dependency is modeled, but the observed variations representing different streets is not modeled as they can not be identified reliably from the large, but limited, measurement datasets.

In this paper, a novel street-by-street (SbS) PL model for UMi environments is presented that fully takes into account the PL non-stationarities. The PL is parametrized separately for each street, and thus the model represents the local PL. The model parametrization is based on a large calibrated ray-tracing (RT) simulation dataset with a total of 11 BS locations and over 60000 PL data points in an UMi street canyon environment at 28 GHz.[1] The model aims to represent the most significant correlations between the parameters for distance dependent PL and the shadow fading as well as the most important geometrical parameters describing the street orientation and the distances from the BS to the street corners and to the MS.

The remainder of the paper is organized as follows: Section II provides a review of standard path loss modeling methods and the way their parameters are extracted from measurements (or simulations). Section II-A introduces the typical $\alpha\beta$- and close-in (CI) reference models and an example of a deterministic street canyon PL model [16] is introduced in Section II-B. In Section III, the ray-tracing datasets and the parametrization for the typical $\alpha\beta$- and CI models are given. The new SbS PL model is given in Sections IV-VI. Section VII will benchmark the proposed SbS model with the $\alpha\beta$- and CI models (parametrized in Section III) as well as with the deterministic model of [16]. Finally, conclusions are given in Section VIII.

[1]While officially 28 GHz band is not part of the mm-wave band (30 GHz - 300 GHz) it is close enough that it is often considered part of it in the literature.

II. Path Loss Models

The local (instantaneous) channel gain, whose inverse is the path loss, can be modeled as the product of three factors: (i) the distance-dependent expected path gain, whose inverse is the expected path loss $\overline{PL}(d)$, (ii) a random variable representing shadowing S, and (iii) a random variable representing small-scale fading (we assume in the sequel that small-scale fading is averaged out, e.g., through the use of averaging with a sliding window). In other words, on a dB scale, the received power P_{RX} can be written as

$$P_{\mathrm{RX}} = P_{\mathrm{TX}} + G_{\mathrm{RX}} + G_{\mathrm{TX}} - PL(d), \tag{1}$$

where G_{RX} and G_{TX} are the receiver (RX) and transmitter (TX) antenna gains, respectively, and P_{TX} is the transmitted power. The path loss $PL(d)$ can be written as

$$PL(d) = \overline{PL}(d) + S. \tag{2}$$

To simplify the discussion, we will henceforth use notation suitable for a downlink scenario (BS as TX, MS as RX), though of course, the PL model is equally valid for the uplink.

The shadowing is usually modeled as a log-normal process, i.e., Gaussian distributed around the mean with a standard deviation σ (again on a dB scale), and autocorrelation function $h(\Delta d)$ describing the correlation of S between two points separated by distance Δd. The autocorrelation function is parametrized with a correlation distance d_{cor} so that S is considered correlated for locations separated by less than the correlation distance. The most common autocorrelation model is a decaying exponential function of the distance separation [28], [29]:

$$h(\Delta d) = \exp(-\Delta d/d_{\mathrm{cor}}), \tag{3}$$

where Δd is the distance separation between MS locations in two-dimensional space, i.e., the xy-plane. Shadow fading within the distance separation less than d_{cor} has correlation $> 1/e \approx 0.36$. Many more detailed shadow fading correlation models have been suggested, see [29] for a survey. We will use the model (3) for further discussion in this paper, but note that our methodology is just as applicable to more involved shadowing models.

A. Typical $\alpha\beta$- and CI Models

The distance dependent expected path loss $\overline{PL}(d)$ is commonly modeled on a dB-scale with the so-called $\alpha\beta$-model, e.g., [10], [30], [31],

$$\overline{PL}_{\alpha\beta}(d) = 10\cdot\alpha\cdot\log_{10}(d/\mathrm{d}_0) + \beta, \tag{4}$$

where α is the PL slope and d_0 is the reference distance. This reference distance can be chosen in various ways, e.g., the smallest distance for which measurements exist, the Rayleigh distance of the transmit antenna, or a fixed value such as 1 m. The parameter β is the offset of the path

loss fitting curve at the reference distance. The CI model, e.g., [13], [14], [19], [20], [32], in which $\overline{PL}_{CI}(d)$ is fixed to the value of the free-space path loss (FSPL) at the reference distance FSPL(d_0), is given as

$$\overline{PL}_{CI}(d) = 10\cdot\overline{n}\cdot\log_{10}(d/d_0) + \mathrm{FSPL}(d_0), \quad (5)$$

where $\overline{n}$ is the path loss exponent. The CI model expected PL equation is a simpler one than the $\alpha\beta$-model as it has only one free parameter. The reference distance is often chosen to be 1 m. The parameters (α and β, or $\overline{n}$) can be obtained as a simple least-square fitting to an ensemble of measurement points obtained from a large area. The σ can then be calculated from the variations of the small scale averaged (SSA) path loss around the $\alpha\beta$- or CI model.[2]

It is customary in PL evaluations that all PL data are considered as part of the ensemble to which the fitting (4) or (5) is done. In particular, in an urban cellular scenario all the data from all the streets, and possibly from many cells, are collected together for the dB-over-$\log_{10}(d/d_0)$-fitting. If, and only if, the PL and the shadowing statistics are stationary, i.e., depend only on the distance between TX and RX, but not on their absolute location, then the variance computed this way is identical to the true shadowing variance, where we define the true shadowing as the variations of the (small-scale averaged) channel gain around its local mean. This implies also that $\overline{PL}(d)$ be the same for every route. If the statistics are not stationary, no such equivalence holds. In that case, this deviation is different from the *true shadowing*, so we henceforth call it the root-mean-square deviation, RMSD.

In this work, the typical $\alpha\beta$-model (or CI model) is considered fully parametrized when α, β, RMSD, and d_{cor} (or $\overline{n}$, RMSD, and d_{cor}) are known for both LOS and NLOS conditions.[3] Reference distance $d_0 = 1$ m, in (4)-(5), and the exponential autocorrelation function (3) are used. In Section III, these models are parametrized for a 28 GHz UMi dataset, and in Section VII used as examples of typical models for the purpose of benchmarking against our model.

Various other PL model extensions and modifications of the basic model have been proposed, for example (i) the breakpoint model, in which $\overline{PL}(d)$ is characterized by a slope α_1 up to a breakpoint distance, and by a slope α_2 at distances beyond that [19]–[21], (ii) probabilistic LOS/NLOS models [10], [13], [19], [20], in which separate fits according to (4) or (5) are obtained for MS locations that are in LOS or NLOS, respectively, and a distance-dependent probability for being in LOS is used for each MS location during the simulation, and (iii) distance dependent RMSD [15], [19], [20]. All of these modifications, while important in their own right, do not significantly impact our discussion below, and in order to simplify notation, we will in this paper assume the validity of the $\alpha\beta$-model (4) as the starting point for the proposed SbS PL model in Section IV.

[2]Note that an alternative formulation is possible; optimizing the log-likelihood function [16], [30], [31]. This can provide slightly improved results under some circumstances, but again does not impact the basic issues discussed here.

[3]Some popular PL models ignore the correlation properties of shadow fading (or RMSD).

B. Deterministic Models

Besides the above models, various street canyon PL models have been proposed, e.g., [16], [17], [33]–[37]. Some are based on simplified ray tracing, e.g., [33], [34]. Also, models including some geometrical parameters and statistical distributions for the shadow fading have been proposed, e.g., [16], [17], [35]. While some of these models include some geometrical parameters, they are deterministic models without the random variations seen in the presented PL-model parameters in this paper.

In this paper we use [16] as an example of deterministic 28 GHz UMi street canyon PL model. It is a frequency-agile path loss model for urban street canyons from 0.8 to 60 GHz based on the ITU-R M.2135 UMi model [35]. The LOS model is an extended ITU-R M.2135 model with expected PL before breakpoint $\overline{PL}_{LOS1}$ and after breakpoint $\overline{PL}_{LOS2}$ at 28 GHz

$$\overline{PL}_{LOS1}(d) = 22\cdot\log_{10}(d/1\text{ m}) + 59.1, \quad (6)$$

$$\overline{PL}_{LOS2}(d) = 40\cdot\log_{10}(d/d'_{BP}) + \overline{PL}_{LOS1}(d'_{BP}), \quad (7)$$

and the breakpoint is

$$d'_{BP} = \frac{(h_{BS} - 1\text{ m})(h_{MS} - 1\text{ m})}{0.0048\text{ m}}, \quad (8)$$

where h_{BS} is the BS height and h_{MS} is the MS height. The LOS shadow fading standard deviation is 2.66 dB. The NLOS model is a simplified ITU-R M.2135 model with expected PL at 28 GHz

$$\overline{PL}_{NLOS}(d_1, d_2) = \overline{PL}_{LOS}(d_1) - 12.5\cdot n_j + 10\cdot n_j\cdot\log_{10}(d_2/1\text{ m}) + 17.1, \quad (9)$$

where $n_j = \min(2.8 - 0.0024\cdot d_1/1\text{ m}, 1.84)$, d_1 and d_2 are the distances from the BS to an intersection of streets and from the MS to the intersection. The zero-point of distance d_2 is in the middle of the intersection [35], i.e., the street corner, and the first NLOS point, is at $d_2 = W/2$, where W is the street width. The NLOS shadow fading standard deviation is 2.94 dB. Further details of this model can be found in [16], [35]. This model is used as an example of a deterministic street canyon model for the purpose of benchmarking against our model in Section VII.

III. Simulated Channel Data and Typical Model

A. PL Data

The typical $\alpha\beta$- and CI models (Section II-A) and the SbS model (Section IV) are parametrized based on calibrated 28 GHz ray-tracing simulations in the urban street canyon environment of New York City (NYC), NY, USA. The main motivation to use ray tracing, instead of channel measurements, is the ability to obtain much larger datasets than would be practically feasible to measure. The dataset has in total 60610 data points and 11 BS locations. The environment can be described as street canyon UMi environment with BS height of 10 m above ground, which is less than the height of the surrounding rooftops. The MS locations were placed at height of 1.5 m above the ground on a rectangular grid within a 590 m $\times$ 450 m area, with 5 m $\times$ 5 m meter gridpoint spacing, only considering outdoor MS deployment.

The 3D building database covers an area that is about 100 m larger in every direction than the area covered by the grid-points; thus reflections from buildings outside the coverage area are included. For simplicity, scattering objects such as cars, people, signs, and billboards are not considered. The typical building height in this area is from 20 to 50 m and street width is from 15 to 30 m.

The parameters for ray-tracing simulation and environment description are set to the values used in [19] and [20]. All paths are modeled by reflection, diffraction, and penetration based on the geometrical optics (GO) and uniform theory of diffraction (UTD) using the ray-tracing software Wireless In-site by REMCOM [38]. In each ray, at most twelve reflections, two penetrations, and a single diffraction are considered as the attenuation by multiple diffractions and combination of reflection and diffraction at mm-wave frequencies is severe [39]. In the geographical model, all buildings and the ground are assumed to be made of concrete and wet earth, respectively [40]. At each combination of BS and MS, at most 40 rays and their signal power, phase, propagation time, direction of departures (DoDs) and direction of arrivals (DoAs) for both azimuth and elevation are collected in descending order of received power within 250 dB per-path path loss. The received power of each MS point is calculated by summing all path powers, and each sample is categorized as LOS or NLOS according to whether visual LOS exists.

The results of the ray tracing are validated by a comparison with measurements in [19]. The pointwise comparison between the measurement and ray-tracing simulations shows some deviations. However, the path loss models derived from these values show reasonable agreement [19]. This is an effect commonly observed in ray tracing, and could only be eliminated by a much more detailed database including small objects. A good statistical match, i.e., similar PL model parameters, is commonly seen as validation of the PL model parameters despite the deviations in the pointwise comparison between the measurement and ray tracing. The SbS PL model, developed in this paper, describes the PL statistics on a street-by-street level. A proper validation of the ray-tracing results by measurements on a street-by-street level requires considerably larger measurement campaigns, which are unfeasible with currently available high-dynamic-range mm-wave channel sounders. Nevertheless, in this paper this ray-tracing PL data is used to develop the new SbS PL modeling principle, while the particular parametrization needs further validation in future.

The measurement results used in the validation have the highest measured PL at about 150 dB [19]. Therefore, in this work PL values above a 160 dB-limit are not used as such high values are not validated. With this limit there are 29755 data points, i.e., about half of the original 60610 data points are now considered to be in outage.

Ray-tracing simulations of Daejeon, Korea, are used as an example of another similar environment [1], [19]. The Daejeon dataset has one BS location. The BS height is 16 m, typical building height is from 10 to 15 m, and typical street width is about 10 to 20 m. The BS is placed below the building rooftop level of a 25 m high building. The MS locations were placed at mobile heights of 1.5 m above the ground on a 1 m × 1 m rectangular grid within a 200 m × 200 m area, only considering outdoor MS deployment. As in the case of the NYC building database, the MS deployment area is smaller than the building database area. This dataset is only used to validate the model derived from the NYC simulations. Also, this smaller dataset is used to illustrate the propagation physics that motivated our SbS PL model [1].

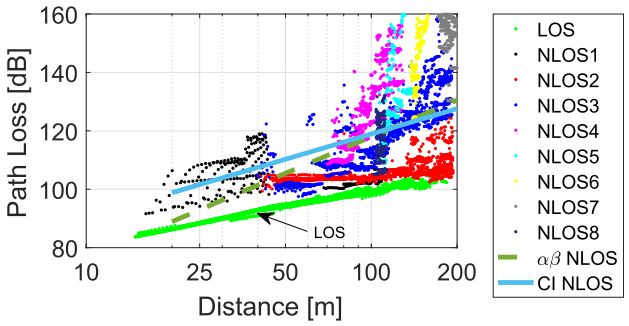

Fig. 1. PL as a function of link distance in LOS and NLOS in the Daejeon dataset. Different colors indicate streets with same colors as in Fig. 2. The typical $\alpha\beta$ (dash line) and CI (solid line) model fitted expected NLOS PL lines are shown and the parameters are listed in Table I.

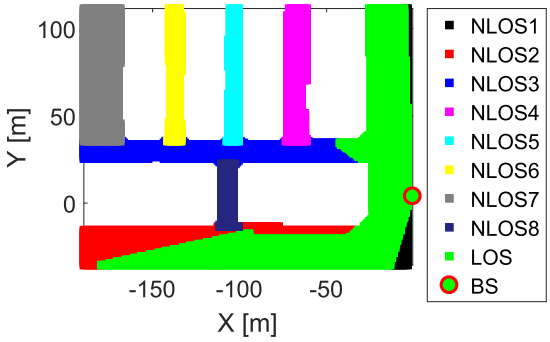

Fig. 2. LOS, NLOS, and base station locations in the Daejeon dataset. The NLOS streets are color coded with different colors for each street and LOS area is green.

TABLE I
PARAMETERS FOR THE TYPICAL $\alpha\beta$- AND CI MODELS: 28 GHZ UMI

	α	β	$\overline{n}$	RMSD	d_{cor}
NYC LOS $\alpha\beta$	1.44	68.8	-	2.11	17
NYC NLOS $\alpha\beta$	3.01	60.2	-	15.2	86
NYC LOS CI	-	-	1.80	2.51	30
NYC NLOS CI	-	-	2.96	15.2	86
Daejeon LOS $\alpha\beta$	1.79	63.6	-	0.56	8
Daejeon NLOS $\alpha\beta$	4.16	34.8	-	14.6	50
Daejeon LOS CI	-	-	1.91	0.64	15
Daejeon NLOS CI	-	-	2.88	14.8	50

B. Propagation Physics

We now use ray-tracing results from the Daejeon dataset to illustrate the points made in Sections I-II, and to motivate an alternative PL model based on simulated propagation physics [1]. Fig. 1 shows the PL in UMi as a function of MS-BS distance for a NLOS scenario. Ignoring for the moment the color coding, we can see that a linear fit with $\alpha \approx 4$ ($\overline{n} \approx 3$) describes the mean. We also see that the deviation

of the measured points around this mean increases drastically with distance, from ±8 dB at 20 m to ±30 dB at 200 m. If we assume a distance-independent standard deviation (as is done in existing PL models), the standard deviation is about 15 dB with both the $\alpha\beta$- and CI models. As we will see below, this deviation is different from the true shadowing, therefore, we call it RMSD.

Let us now turn to a more local interpretation: different streets are signified by different colors in Figs. 1-2. Thus, an MS moving along a trajectory within one street would only experience PL of that particular color. We can clearly observe that different streets have greatly differing PL coefficients: e.g., points on the red street (NLOS2) show a negligible slope while the dark blue street (NLOS8) corresponds to an almost vertical line in Fig. 1. These effects can be easily explained by the dominant propagation physics. The red area is part of the street that also contains LOS components over the roof of a relatively low building; this means that waves are very efficiently coupled into this area, typically via one or more reflections. The wave guiding effect ensures that the effective PL slope is even less than in a free-space propagation scenario (remember that the PL exponent for a perfect waveguide is 0). Thus, even though points in the red area have a distance from the BS ranging from 40 m to 200 m, the PL hardly changes. Next, note the blue area, NLOS3. This street is parallel to the red street. However, the coupling angle is slightly different, and the building structures are such that only a small area is in LOS. For this reason, the coupling into the waveguide is less efficient, and waves have to undergo a large number of reflections on their way to the far-away points in the canyon. Due to the lossy nature of the waveguide walls, the blue points show a significantly higher slope than the red points. We finally observe the dark blue points, NLOS8. All points in that street are at approximately the same distance to the BS. Waves mostly propagate from the BS, through the red and blue streets, and from there are coupled into the dark-blue street. Points that are midway between the blue and red street, either require a diffraction with a large angle (and thus high loss) or a diffraction with a smaller angle followed by multiple reflections. Points near the junction between dark blue and red (or blue) street have a much smaller loss. Thus, we see a wide range of PL, even though the Euclidean distance from BS to MS hardly varies. This provides us with the important insight that Euclidean distance between the BS and MS is not necessarily a dominant parameter of the PL. Similar, though slightly less pronounced, effects can be observed in all the other vertical streets. This indicates that the street orientation (relative to the BS position) has an important impact on the PL parameters.

Relating these physical insights now to the modeling approach of Section II, we find that the PL statistics are extremely non-stationary. The difference in PL between two points clearly depends not only on the distance between the points but also on the absolute position - most notably, which street the two points are in. We also see that the reason for the large deviation between "mean" PL of the cell, and the locally simulated points, is mostly due to the fact that different streets have different slopes. This also explains the distance dependence of the RMSD. It is not the actual shadowing along a trajectory that increases in variance, but rather the different slopes of the expected PL in each street cause a stronger variation between the smallest and largest PL at larger distances. For LOS, on the other hand, the difference is much smaller; the LOS (green) areas of both the "horizontal" street and the "vertical" street (in Fig. 2) lead to almost identical PL distribution.

C. Typical $\alpha\beta$- and CI Model Parameters

The parameters for the typical $\alpha\beta$- and CI model parameters are derived for Daejeon and NYC datasets. The resulting 28 GHz UMi PL model parameters for LOS and NLOS are presented in Table I. The number of data points in the NYC dataset, with PL $<$ 160 dB, is 5343 and 25512 in LOS and NLOS, respectively. The maximum link distances are about 600 m. The number of data points in the Daejeon dataset, with PL $<$ 160 dB, is 5099 and 5465 in LOS and NLOS, respectively. The maximum link distances are about 200 m. Comparing the parameters for NYC and Daejeon, we see that they are quite similar, especially with the CI model.

A very large RMSD $\approx$ 15 dB is found for NLOS.[4] As pointed out in the previous section, and in our conference paper [1], the large NLOS RMSD is mostly due to differences between PL on different streets rather than the true shadowing being so large. Similarly, although to a lesser extent, the LOS RMSD ($\sigma = 2.11$ dB) is partly due to differences between streets.

Analyzing the 11 BS locations in NYC separately we observe different PL parameters for each BS location. For example, the NLOS path loss slope α varies between 2 and 5, the RMSD is between 12 and 18 dB, and the RMSD correlation distance is between 28 and 50 m. In LOS, α varies between 1.3 and 1.8, the RMSD is between 1.2 and 3 dB, and the RMSD correlation distance is between 8 and 45 m. The CI model PL exponent $\overline{n}$ is quite stable due to the fixed reference point at 1 m, but the RMSD and RMSD correlation distance varies as much as with the $\alpha\beta$-model. This clearly shows the non-stationarity of the PL parameters also from cell to cell and is consistent with the findings of [22]. However, the current paper is focused on the street-by-street level model and therefore the variations between BS locations are outside its scope.

IV. Street-by-Street Path Loss Equations

As a first step in our modeling, we extract the distance dependent expected path loss $\overline{PL}(d)$ and shadow fading parameters separately for each street or part of a street. The same street can be, e.g., partly in LOS and partly in NLOS, or divided into two NLOS areas. In this context we use the word *street* for any partition of the urban street grid, including, e.g., park or an open area. For example in the case when the BS is located at the center of an intersection of two streets there are *four LOS streets* pointing away from the BS.

[4]This is partly because of the relatively high simulated PL levels up to 160 dB. In fact, both of the ray-tracing datasets include PL values up to 220 dB, and if all data points are included, the NLOS RMSE would be over 20 dB for both datasets and both models.

In LOS, the distance is defined, just as in the traditional model, as the Euclidean distance between BS and MS. In NLOS, the distance is measured along the street canyons as the total distance between BS and MS *approximately* following the *dominant propagation mechanism*, i.e., shortest route favoring LOS areas and minimizing the number of corners.[5] More discussion and illustration on how a street grid is divided into LOS and NLOS streets is given in Section V.

For a given BS location, we now index the streets according to the number of sharp corners the signal has to turn in order to reach the MS. The LOS is $n = 0$ and the NLOS street is $n = 1$. Furthermore, there might exist a NLOS street with $n = 2$ from which the shortest distance to LOS goes around two street corners. In a general case, the SbS PL equation is written for street n with the known PL equation for the previous street $n - 1$ that might be a NLOS or LOS street. Finally, we note that moving from a street with index $n - 1$ to index n incurs a *corner loss*. In our model we describe this loss as a jump in the expected path loss, though in reality of course there is a smooth transition related to the specifics of the propagation process that couples the radiation into the street.

Let us then first write the typical $\alpha\beta$-PL model for NLOS street n using corner loss Δ_n defined in dB as:

$$\overline{PL}_n(d_n) = 10 \cdot \alpha_n \cdot \log_{10}(d_n/1\text{ m}) + \beta_n. \quad (10)$$

$$\Delta_n = \overline{PL}_n(d_c) - \overline{PL}_{n-1}(d_c), \quad (11)$$

$$\Delta_n = 10 \cdot \alpha_n \cdot \log_{10}(d_c/1\text{ m}) + \beta_n - \overline{PL}_{n-1}(d_c). \quad (12)$$

Substituting β_n from (12) into (10) we get the PL-model for NLOS street n

$$\overline{PL}_n(d_n) = 10 \cdot \alpha_n \cdot \log_{10}(d_n/d_c) + \Delta_n + \overline{PL}_{n-1}(d_c), \quad (13)$$

where Δ_n is corner coupling loss at the corner of street n, d_n is the total distance from the BS to the MS along the street canyons, d_c is the total distance from the BS to the n-th corner.

In order to maintain meaningful physical interpretation of the corner coupling loss and PL slope, additional conditions are enforced[6]:

$$\Delta \geq 0, \quad (14)$$

$$\alpha \geq 0. \quad (15)$$

Similar formulations for LOS give:

$$\overline{PL}(d) = 10 \cdot \alpha \cdot \log_{10}(d/1\text{ m}) + \beta. \quad (16)$$

$$\overline{PL}(d) = 10 \cdot \alpha \cdot \log_{10}(d/1\text{ m}) + \Delta + \text{FSPL}(1\text{ m}), \quad (17)$$

where Δ is an offset vs. free space path loss (FSPL) at 1 m reference distance. Unlike the NLOS case, the LOS-Δ does not have a clear physical meaning and it should be seen only as a fitting parameter; in one variant of the model, it can be forced to 0. In addition to the parameters in (13) and (17), the shadow fading standard deviation σ and correlation distance d_{cor} are needed for all LOS and NLOS streets.

[5]In this work we do not assume that the path of dominant propagation mechanism is known. Alternatively, if such information is available, NLOS streets can be defined along such paths.

[6]Negative α in NLOS is in fact physically possible if strong propagation path(s) do not follow the shortest route. As negative α can cause unphysically low PL, the PL on streets with decreasing expected value of PL are approximated with $\alpha = 0$.

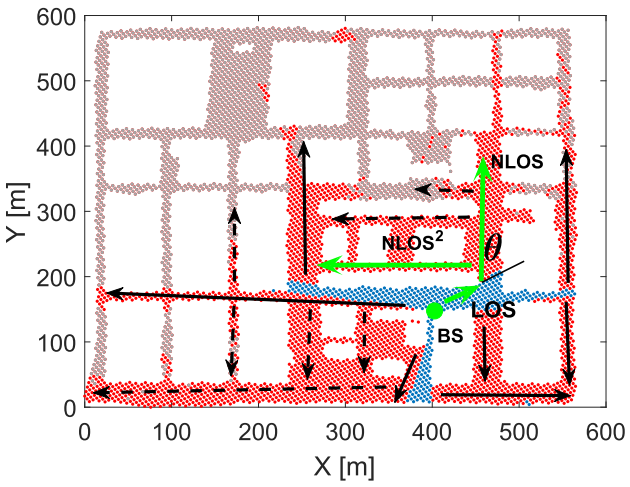

Fig. 3. MS locations in LOS (blue), NLOS (red), and *outage* (grey), i.e., location with $PL > 160$ dB. The BS is shown in green. One LOS street, NLOS street, and NLOS street behind two corners, i.e. NLOS^2, are chosen as examples (green arrows). The thin black arrows show the directions of all the NLOS streets and the dash line arrows show the NLOS^2 streets.

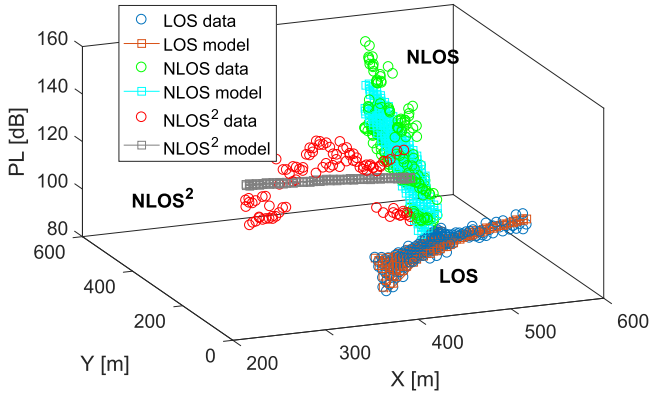

Fig. 4. PL and fitted PL models for the three chosen examples (BS and MS locations illustrated in Fig. 3).

V. Street-by-Street Model Parametrization

We now describe the SbS PL model parametrization by means of examples of a LOS street, a NLOS street, and a NLOS street behind two corners, called NLOS^2, see Figs. 3-4. Fig. 3 shows a map of MS locations for one of the 11 BS locations in the NYC dataset (see Section III and Fig. 9). The locations are divided into LOS, NLOS, and outage locations, i.e., NLOS locations with $PL > 160$ dB. The exact PL is not known for the outage location and, for simplicity, are excluded from the analysis.[7] The BS coordinates are $(x_{\text{BS}}, y_{\text{BS}}, z_{\text{BS}})$ and the MS coordinates are $(x_{\text{MS}}, y_{\text{MS}}, z_{\text{MS}})$. The parametrization starts with the LOS streets. In this case, there are three LOS streets within the simulation area: streets going $+y$- and $\pm x$-directions from the BS. The NLOS locations are divided into NLOS and NLOS^2 streets, as illustrated in Fig. 3. Firstly, every street corner from a LOS area begins an NLOS street. The NLOS^2 streets are then the streets

[7]The data from the outage locations could be taken into account as in [30].

starting from an NLOS street.[8] After this, almost all points are assigned to a street (or two, in case of intersections) and the rest of the data is excluded due to small sample size of such areas.

Let us examine more closely one series of LOS, NLOS, and NLOS^2 streets (shown with green arrows in Fig. 3). The PL values and the fitted models are presented in Fig. 4. The parametrization goes step-by-step starting from the BS as follows:

1) LOS: This LOS street includes all LOS MS locations with $x_{\text{MS}} > x_{\text{BS}}$. The distance d for (17) is the Eucledian distance between the BS and the MS locations. The model (17) is fitted with least-square error fitting and the resulting parameters are: $\alpha = 1.6$ and $\Delta = 5.9$. The variation from the expected PL model, i.e., the shadow fading, is parametrized by a shadow fading standard deviation $\sigma = 1.2$ and correlation distance $d_{\text{cor}} = 7.2$ m.
2) NLOS: This street corner is $d_c = 71$ m away from the BS. The distance d_c is calculated only from x- and y-coordinates. The LOS street PL model at the street corner gives $\overline{PL}_{n-1}(d_c) = 97$ dB. The distance along an NLOS street, d_n in (13), is approximated as d_c plus the difference of the y-coordinates of the MS and the corner. Fitting the model to this street gives: $\alpha = 6.2$, $\Delta = 0$, $\sigma = 5.9$, and $d_{\text{cor}} = 7.3$ m. The corner angle θ, as defined in Fig. 3, is $\approx 52°$. The d_c and θ are used in Section VI to model the dependence of the PL parameters on these geometrical parameters.
3) NLOS^2: The street corner is a total of $d_c = 93$ m away from the BS, which is the combination of the 71 m plus 22 m along the NLOS street - we stress again that this distance is different from the Euclidean distance. The NLOS model gives $\overline{PL}_{n-1}(d_c) = 104$ dB at the street corner. The distance along a NLOS street, d_n in (13) is now calculated as $d_c = 93$ m plus the difference of the x-coordinates of the MS and the corner. The model fitting gives $\alpha = 1.1$, $\Delta = 17$, $\sigma = 11$, and $d_{\text{cor}} = 15$ m. The corner angle between the NLOS street and the NLOS^2 street is $\theta = 84°$.

The resulting street-by-street parametrization of the 11 BS locations in the NYC dataset give the parameter statistics used for the model. In total 28 LOS, 108 NLOS, and 56 NLOS^2 streets are parametrized and the statistics are presented in Table II. In addition to mean, standard deviation, minimum, and maximum values for α, Δ, σ, and d_{cor}, also probability of zero values $p(0)$ are given for α and Δ. Streets with less than 25 MS locations are not included. Also, two LOS streets are excluded as outliers, due to abnormally large d_{cor}.[9]

These parameter statistics clearly show that the RMSD variations of the typical $\alpha\beta$- and CI models (Table I) are in most cases much larger than the signal variations along a route of the MS. Again, this comparison confirms the observation in Section III-B, that the typical model RMSE deviation is different from the true shadowing along a trajectory. Especially in NLOS the PL behaves radically differently on different streets, as shown by the large standard deviations of the parameters. The wide range of the PL parameters clearly motivates modeling the PL behavior with statistical distributions in order to capture the observed range of the parameter statistics.

[8]In general, there are a few optional routes from BS to a NLOS^2 street through different NLOS streets. In this paper, NLOS^2 street starts from the intersection closest to the BS.

[9]Abnormal values are excluded due to their disproportionately large effect on the statistics.

TABLE II
PARAMETER STATISTICS: MEAN, STANDARD DEVIATION, MINIMUM, MAXIMUM, AND PROBABILITY OF A ZERO VALUE $p(0)$

		LOS	NLOS $\theta < 75°$	NLOS $\theta \approx 90°$	NLOS^2
α	mean	1.4	3.6	14	11
	std	0.21	3.2	13	17
	min	0.94	0	0	0
	max	1.73	11	54	112
	$p(0)$	0	0.13	0.01	0.20
Δ	mean	8.4	4.4	17	8.3
	std	3.3	4.9	10	9.1
	min	1.3	0	0	0
	max	15	15	35	38
	$p(0)$	0	0.39	0.05	0.21
σ	mean	1.2	4.9	8.2	7.5
	std	0.44	2.5	2.8	2.9
	min	0.47	1.1	1.7	1.36
	max	2.3	9.3	22	15
d_{cor}	mean	7.2	6.0	7.8	8.7
	std	3.7	4.5	4.4	7.8
	min	1.9	0.08	0.09	0.09
	max	18	17	22	43

TABLE III
THE STREET-BY-STREET PATH LOSS MODEL PARAMETER EQUATIONS

LOS
$\alpha = 1.4 + 0.21 \cdot X_\alpha$
$\Delta = 30 - 15 \cdot \alpha$
$\sigma = 1.2 + 0.44 \cdot X_\sigma$
$d_{\text{cor}} = 7.1 + 4.3 \cdot \sigma + 3.2 \cdot X_{dcor}$
NLOS, $\theta < 75°$
$\alpha = 0.92 + 0.093 \cdot \theta + 1.6 \cdot X_\alpha$
$\Delta = 3.6 + 4.7 \cdot X_\Delta$
$\sigma = 4.9 + 2.5 \cdot X_\sigma$
$d_{\text{cor}} = 5.8 + 4.6 \cdot X_{dcor}$
NLOS, $\theta \approx 90°$
$\alpha = -2.3 + 0.089 \cdot d_c + 8.2 \cdot X_\alpha$
$\Delta = 17 + 9.7 \cdot X_\Delta$
$\sigma = 8.1 + 2.8 \cdot X_\sigma$
$d_{\text{cor}} = 7.6 + 4.2 \cdot X_{dcor}$
NLOS^2
$\alpha = 12 + 12 \cdot X_\alpha$
$\Delta = 9.0 + 9.5 \cdot X_\Delta$
$\sigma = 7.6 + 2.8 \cdot X_\sigma$
$d_{\text{cor}} = 8.5 + 7.1 \cdot X_{dcor}$

VI. STREET-BY-STREET PATH LOSS MODEL

The SbS PL model describes how to generate the PL-equation parameters (α, Δ, σ, and d_{cor}) for the LOS, NLOS, and NLOS^2 streets as presented in Table III. These equations are formulated based on cross-correlations between the parameters, and in the NLOS cases also with the geometrical parameters d_c and θ. Only correlations > 0.50 (or < -0.50) are modeled, otherwise the parameters are assumed to be independent. The cross-correlations between the parameters

TABLE IV

LOS: CROSS-CORRELATIONS. α AND Δ ARE VERY STRONGLY CORRELATED AND σ AND d_{cor} ARE STRONGLY CORRELATED

	α	Δ	σ
Δ	**-0.95**		
σ	-0.15	0.08	
d_{cor}	0.07	-0.09	**0.52**

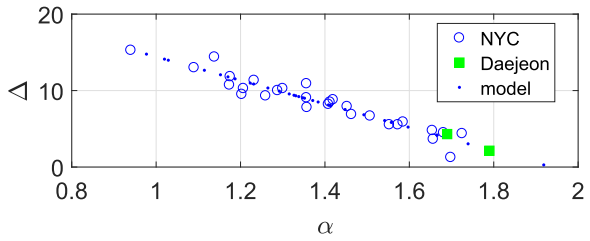

Fig. 5. LOS; Δ and α are very strongly correlated and therefore Δ is modeled as a simple function of α without any variation from the linear line.

are used only to identify which parameters need to be modeled as a function of each other. While the exact approach would be to directly generate correlated Gaussian parameters, for simplicity we use a sequential approach. The parameters are generated in the following order: (i) α, (ii) Δ, (iii) σ, (iv) d_{cor}. The later parameters are allowed to be a function of the earlier parameters. Finally, there is one simple equation for each of the four parameters that approximate the parameter statistics in Table II and the identified strong cross-correlations.

A. LOS

The cross-correlation matrix of the LOS parameters is presented in Table IV. Two strong correlations are observed; between α and Δ and between σ and d_{cor}. As the cross-correlation between α and Δ is close to -1, the Δ is modeled as a simple linear function of α. The LOS street-by-street PL model equations are presented in Table III, where the X are independent random variables following a truncated normal distributions $N(0, 1)$ representing the variation from average values. Δ and σ are in dB and d_{cor} in meter. The α, σ, or d_{cor} are not allowed to be negative, i.e., truncated normal distributions are used.[10]

The α and Δ values from the Daejeon and NYC datasets are presented in Fig. 5. Fig. 5 clearly demonstrates the strong cross-correlation between these parameters. Also, example results from the model equations are presented. The cross-correlation matrix from the model output gives cross-correlation of -1 between α and Δ, 0.49 between σ and d_{cor}, and zero for others.

B. NLOS

The NLOS streets are divided into two groups based on the corner angle of (i) $\theta < 75°$ and (ii) $\theta \approx 90°$. The second group includes all NLOS streets with θ from 75° up to about 100°. NLOS streets with θ far greater than $\theta \approx 90°$ are not present in the NYC (or Daejeon) simulation areas. These streets are

[10]These distributions can be truncated either at zero, as done in this paper, or alternatively with the minimum values observed in the data.

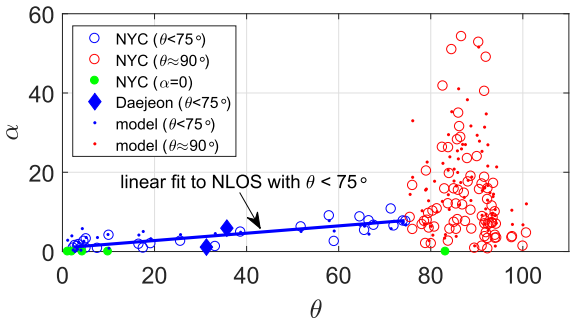

Fig. 6. The NLOS streets are divided into two groups, $\theta < 75°$ and $\theta \approx 90°$, based on the behavior of the PL slope α as a function of the corner angle θ. With $\theta < 75°$, α is strongly correlated with the θ.

TABLE V

NLOS WITH $\theta < 75°$, THE STRONG CROSS-CORRELATION BETWEEN α AND θ IS MODELED

	α	Δ	σ	d_c	θ
α				-0.13	**0.86**
Δ	0.03			-0.21	0.33
σ	0.41	0.15		-0.30	0.33
d_{cor}	0.23	-0.20	0.29	-0.35	0.18

divided into these two groups based on the difference in behavior of the α as a function of θ, shown in Fig. 6. The NLOS α and θ values from the Daejeon and the NYC datasets are presented in Fig. 6, together with examples of the model generated with the same geometrical parameters. Similarly α as a function of the distance from the BS to the street corner d_c is presented in Fig. 7. As shown in Figs. 6 - 7, the model approximates the parameter distributions well. All the comparisons with the data and the model are calculated with the same distributions of the geometrical parameters.

The cross-correlations between α, Δ, σ, d_{cor}, d_c, and θ are shown in Tables V - VI. The streets with $\alpha = 0$ are not used to calculate these correlations nor to derive the following equations for NLOS. The exclusion of these streets is justified by differences in the parameter distributions between streets with $\alpha = 0$ and $\alpha > 0$, and the relatively small sample size of streets with $\alpha = 0$. The inclusion of the streets with $\alpha = 0$ would create correlations that would be due to only one or two streets.[11] Finally, there are 27 NLOS streets with $\theta < 75°$ and 76 with $\theta \approx 90°$ that are used to derive the model equations.

The cross-correlations show that α is a function of corner angle θ when $\theta < 75°$ and a function of the distance to the corner d_c when $\theta \approx 90°$. In both cases all other parameters have relatively low cross-correlations and are modeled as independent random parameters.

The NLOS street-by-street PL model equations are presented in Table III. Truncated normal distributions are used for σ and d_{cor} to ensure non-zero positive values. To be consistent with (14)-(15), negative α and Δ are replaced with zeros. In case of $\theta < 75°$ the model gives 6% and 15% of $\alpha = 0$ and $\Delta = 0$, respectively. In case of $\theta \approx 90°$ the model gives 0% and 2% of $\alpha = 0$ and $\Delta = 0$, respectively. These probabilities

[11]Streets with $\Delta = 0$ are included despite having a similarly low sample size since the streets with $\Delta = 0$ fit well the same distributions that are observed for streets with $\Delta > 0$.

TABLE VI

NLOS WITH $\theta \approx 90°$, STRONG CROSS-CORRELATION BETWEEN α AND d_c IS MODELED

	α	Δ	σ	d_c	θ
α				**0.76**	-0.11
Δ	-0.24			-0.00	-0.05
σ	0.14	0.44		0.38	-0.20
d_{cor}	-0.20	0.10	0.02	-0.08	-0.10

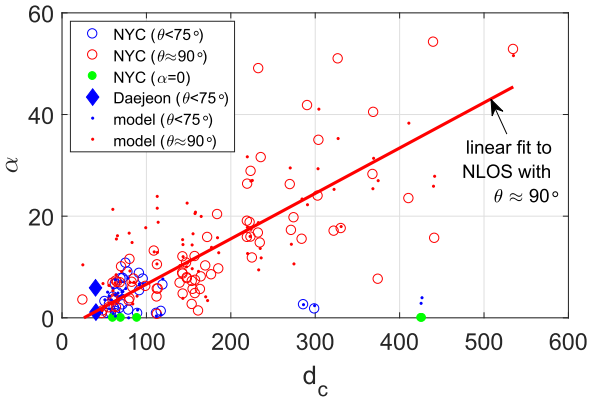

Fig. 7. NLOS; with $\theta \approx 90°$ α is strongly cross-correlated with the distance from the BS to the corner d_c.

match quite well the values in Table II. The cross-correlations between parameters can be calculated from the parameters generated with the model equations using the distributions of the geometrical parameters from the parametrized streets. The model replicates all the modeled strong cross-correlations in Tables V - VI with better than ± 0.05 accuracy.

The relatively low α for NLOS with $\theta < 75°$ clearly illustrates the selection bias for the typical model with the selection of one (or a few) simulation (or measurement) BS location. E.g., if the BS is placed in the middle of the intersection, then the NLOS streets with theta $\theta < 75°$ would be missing and the average α, and average PL, would be higher in NLOS. The SbS model does not suffer from this selection bias as these streets are modeled separately.

C. NLOS ($n = 2$)

The cross-correlations between the parameters of the NLOS^2 streets behind two corners ($n = 2$) are presented in Table VII. Similarly to the case of the normal ($n = 1$) NLOS streets, the streets with $\alpha = 0$ are not used to calculate the correlations or to parameterize the model equations. Therefore, 57 out of the 71 NLOS^2 streets were used, since 14 resulted in $\alpha = 0$. The NLOS^2 parameters are not strongly correlated with each other. None of the parameters are correlated with the corner angle to the NLOS street θ_{n-1} nor with the corner angle from the NLOS street to the NLOS^2 street θ_n.

The NLOS^2 street-by-street PL model equations are presented in Table III. Negative α and Δ are replaced with zeros and the σ and d_{cor} distributions are truncated to ensure positive values. The model generates about 7% with $\alpha = 0$ and 16% with $\Delta = 0$. The NLOS^2 street α and d_c values from the Daejeon and the NYC dataset are presented in Fig. 8, together with examples of the model generated for same

TABLE VII

NLOS STREETS BEHIND TWO CORNERS

	α	Δ	σ	d_c	θ_{n-1}	θ_n
α				0.47	-0.45	0.12
Δ	-0.15			0.02	-0.18	0.22
σ	-0.16	0.45		0.03	-0.05	0.26
d_{cor}	-0.29	-0.01	0.40	-0.17	0.04	0.19

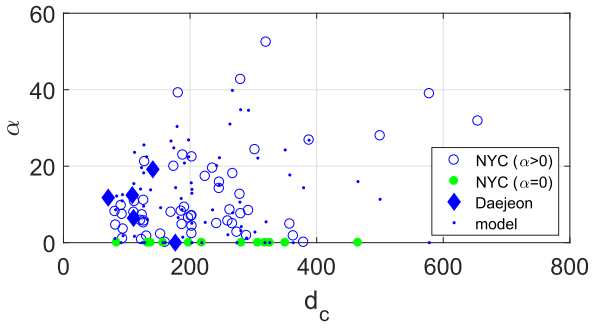

Fig. 8. NLOS^2 streets behind two corners. α as a functions of the total distance from the BS to the corner d_c.

geometrical parameters. As there are no strong correlations, the model approximates all the cross-correlations with zeros. Therefore, the model, e.g., underestimates the correlation between α and d_c. This results from the limit of > 0.50 (or < -0.50) used to determine whether parameters are modeled as independent random parameters.

D. Unrealistic Combinations of Parameters

Sometimes the developed SbS model can produce unrealistic combinations of the PL equation parameters α, Δ, and σ in NLOS or NLOS^2, and thus, unphysical PL values. Two such examples are recognized. Firstly, while it is true that sometimes the expected PL in NLOS is nearly as low as in LOS, such cases always also have small shadow fading variation. Therefore, the combination of large σ with small α and Δ should be avoided or else the NLOS PL can occasionally by clearly lower than in LOS. This requirement can be formulated as[12]

$$\frac{\sigma}{\alpha + \Delta + 1} \leq C_1, \tag{18}$$

where C_1 is the largest observed value in the dataset for the given ratio (disregarding outliers). The "+1" is needed to avoid dividing by zero. The C_1 limits are 0.4, 1.5, and 4.1 in NLOS with $\theta < 75°$, NLOS with $\theta \approx 90°$, and NLOS^2, respectively.

Secondly, high PL values are in general associated with large variations as a function of the distance. Therefore, the combination of small σ, small α, and large Δ should be avoided. This requirement can be formulated as [12]

$$\frac{\Delta + 1}{\alpha + \sigma} \leq C_2, \tag{19}$$

where C_2 is the largest observed value in the data set for the given ratio (disregarding outliers). Again, the "+1" is needed to avoid zero. The C_2 limits are 2.5, 1.9, and 1.9 in NLOS

[12]These ratios have no physical meaning and are used only as numerical tests.

TABLE VIII
DAEJEON STREET-BY-STREET MODEL PARAMETERS

	α	Δ	σ	d_{cor}	n	θ_n	d_c
LOS1	1.8	1.7	0.49	8.5	-	-	-
LOS2	2.1	4.3	0.59	3.2	-	-	-
NLOS2	1.1	8.1	3.1	2.3	1	40	-
NLOS3	5.9	0	6.5	5.8	1	40	-
NLOS4	11	0	7.4	2.5	2	-	71
NLOS5	12	0	9.5	1.7	2	-	109
NLOS6	19	10	5.7	1.8	2	-	141
NLOS7	0	21	7.1	2.2	2	-	177
NLOS8	4.3	4.1	5.9	1.9	2	-	111

with $\theta < 75°$, NLOS with $\theta \approx 90°$, and NLOS^2, respectively. These additional conditions are applied in the comparisons of the data and the model in Sections VI-A - VI-C and in the simulation example in Section VII.

E. Comparison Between Daejeon and NYC Datasets

Only the 11 BS locations from the NYC dataset are used to parametrize the SbS model. Also the streets in the Daejeon dataset, with only one BS, are parametrized for comparison. The SbS model parameters for the Daejeon dataset are presented in Table VIII. The LOS and NLOS areas are shown in Fig. 2. The LOS area is divided into two LOS streets, called LOS1 with $y_{MS} > y_{BS}$ and LOS2 with $y_{MS} < y_{BS}$. NLOS1 is not parametrized due to relatively small area. There are two NLOS streets with $\theta < 75°$, NLOS2 and NLOS3, and five NLOS^2 streets, NLOS4 - NLOS8. The parameters from the Daejeon streets are shown with different markers in Figs. 5 - 8. The parameter statistic from the Daejeon dataset in Table VIII, and from the NYC dataset in Table II, can be compared to see if these two environments are similar.[13] The parameter distributions match quite well[14] with the only exception of larger α and smaller Δ values in LOS streets in Daejeon. Comparison of a few examples from the smaller Daejeon dataset to the larger NYC dataset aims to see if the parameters could be samples from a similar probability distribution. The similarity of the parameter distributions between the Daejeon and the NYC dataset indicates that the proposed SbS model principle is usable also in different urban UMi environments. Further study is needed to derive parametrization for various environments and to study how the differences, e.g., in building height, street width, BS height, etc., might affect the parameter distributions and cross-correlations.

VII. SIMULATION EXAMPLE

In this section, we aim to show that the proposed SbS model improves the spatial consistency compared to the other models, i.e., PL modeling accuracy as the MS moves along a route. Comparison is done with a simulated route in the area of the NYC dataset ray-tracing area with the same BS locations, thus allowing a direct comparison of the original data and the PL behavior predicted by the models. The map, BS locations, and the simulation route are illustrated in Fig. 9. The route is 3690 m long with MS locations every 15 m. A maximum PL level of 160 dB was used to parametrize the SbS model and the typical $\alpha\beta$- and CI models. The same PL cutoff limit is used in these comparisons and PL values over 160 dB are not used, i.e., those locations are in outage without any power value assigned. All the models are assigned the LOS/NLOS condition based on the NYC map and the BS locations as well as all the geometrical parameters needed in the models.

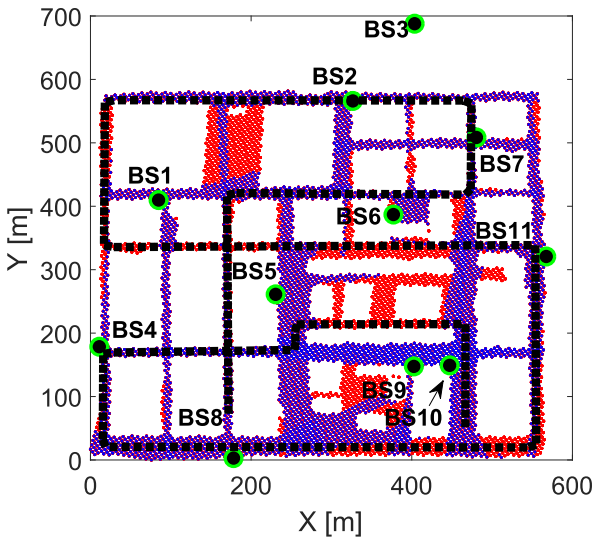

Fig. 9. Simulation route on the NYC map and the 11 BS locations. The route is marked with black dash line. The route starts close to BS8 and ends close to BS10. Blue and red areas are the MS locations. Only outdoor MS locations are simulated. Blue areas are in LOS to one or more BS and red areas are in LOS to none of the 11 BSs. Note that the BS3 is outside the MS location deployment area in the ray tracing but it is within the larger building database area.

The following models are compared:

1) The proposed SbS model as presented in Secs. IV - VI. PL values are not available for MS locations outside LOS, NLOS, and NLOS^2, and those locations are in outage. The geometrical parameters come from the map, i.e, link distance along the street canyons, distance to corner d_c, and corner angle θ.
2) The typical $\alpha\beta$- and CI models with the model parameters as given in Table I. The only geometrical parameter that the typical models use is the link distance.
3) A quasi-deterministic 28 GHz UMi street canyon PL model from [16], presented in Section II-B. This model is used as an example because it has been parametrized for 28 GHz UMi. The main differences to the proposed SbS model are that [16] has been parametrized based on measurements and it does not model the variations in the PL model parameters. Also, [16] has only LOS and single-corner-NLOS, while other MS locations, including NLOS^2, are in outage. The average d_{cor} for LOS and NLOS are taken from the SbS model as [16] does not include shadow fading correlation properties. $d_{\text{cor}} = 7.2$ m is used for LOS. An average of all NLOS and NLOS^2, $d_{\text{cor}} = 7.8$ m, is used for NLOS. BS and MS height and link distances for (6) - (9) are taken

[13]Comparison can be performed only for LOS, NLOS (with $\theta \approx 40°$), and NLOS^2.

[14]Assuming normal distribution, the 95% confidence interval is given by the mean ± 1.96 times the standard deviation.

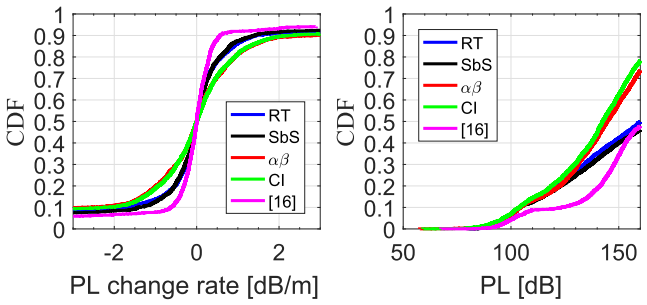

Fig. 10. Comparison of the ray-tracing PL and the models: street-by-street model (SbS), $\alpha\beta$ model ($\alpha\beta$), CI model (CI), and model [16]. Comparison of PL and PL rate of change statistics gathered along the route with all 11 BS.

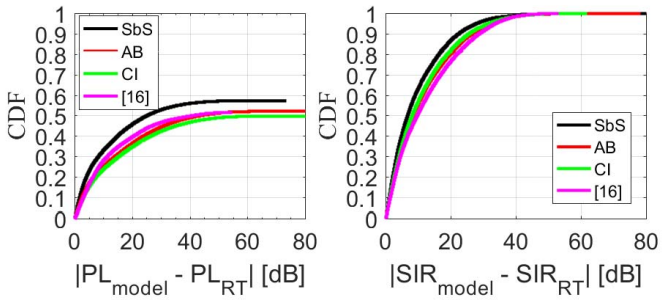

Fig. 11. Comparison of the ray-tracing PL and the models: street-by-street model (SbS), $\alpha\beta$ model ($\alpha\beta$), CI model (CI), and model [16]. Difference between the model and RT; PL and SIR on each point along the route. The PL difference is not calculated for location in which RT or model is in outage, and therefore the CDFs do not go up to 1.

from the map. For simplicity the same street width value $W = 20$ m is used for all streets.

PL statistics along this route are gathered for all the models. Comparison is done based on the PL values, the rate PL changes along the route, and signal-to-interference ratio (SIR). The signal is the strongest received power from BS with the lowest PL and the interference is calculated as the sum of powers from all other BSs. Comparison can be done for statistics for the whole route (e.g., by comparing simulated mean SIR to mean SIR from the model) or for every point along the route. Comparison of PL and SIR values from the models to the original RT data gives statistics on the prediction error locally for all points.

Cumulative distributions functions (CDFs) of PL values and PL rate of change, given in dB/m, are shown in Fig. 10. These statistics are gathered along the route from all 11 BS and several runs of the models. As depicted, the proposed SbS model clearly gives the best match to the RT data. The SbS model gives the best fit also in the tails of the CDFs. The model from [16], has been parametrized based on different data and gives different PL value statistics due to differences in the levels of expected PL. Therefore, the more important comparison is in the PL rate of change, where we can see that the model [16] clearly underestimates how fast the PL changes locally. The typical $\alpha\beta$- and CI models give similar results and both overestimate it. The effects of large RMSD values can be observed in Fig. 10. With relatively high PL levels, typical in NLOS, PL along many NLOS streets changes fast, with large PL slope, as explained in Section III-B.

Furthermore, these models have a simple expected PL equation which only depends on the distance between the BS and MS and do not take into account the street grid geometry. Mean and standard deviation statistics of SIR along the route are compared in Table IX. Again, the proposed SbS model gives the best match to the values calculated directly from the ray-tracing data. Comparison of PL and SIR values on each point along the route provide statistics on the difference between the original ray tracing and the values predicted by the models presented in Fig. 11. This kind of local difference is a good measure of the spatial consistency. As shown in Fig. 11, the proposed SbS model provides smaller differences to the ray-tracing data for both PL and SIR. Note that the models do not try to replicate the ray-tracing data, rather the model should have similar statistics along the route as well as locally.

TABLE IX

MEAN AND STANDARD DEVIATION OF SIR ALONG THE ROUTE WITH ALL 11 BS. RAY TRACING (RT), STREET-BY-STREET MODEL (SBS), $\alpha\beta$ MODEL ($\alpha\beta$), CI MODEL (CI), AND MODEL [16]

Model	mean SIR [dB]	std SIR [dB]
RT	15.8	14.2
SbS	15.7	13.0
$\alpha\beta$	14.1	11.7
CI	13.6	11.3
[16]	23.7	16.9

The comparison presented in this section clearly shows that the SbS model provides improved accuracy both locally as well as on the statistics along a long route. The comparison is conducted between the models and the ray-tracing dataset used in this paper to parametrize the proposed model. Therefore, the modeling principle is proven to be able to accurately model the PL behavior in this dataset in a spatially consistent manner. It is important to note that this particular parametrization has not been validated for all street canyon environments, e.g., in different cities; this will require comparison to different datasets that are not used for parametrization. Preferably the validation should be done with measured PL datasets.

VIII. CONCLUSION

In this paper we have analyzed the traditional method of PL modeling that provides a straight-line fit (on a dB-over-$\log_{10}(d/\mathrm{d}_0)$ scale) to all PL values measured in a cell. We found that in urban environments, the deviations from the PL fit can be ascribed to two distinct effects, namely (i) "true" shadowing, i.e., variations of the received power around the distance-dependent mean as the MS moves on a trajectory down a street canyon, and (ii) variations of the offset and the slope of the straight-line fit *between* different street canyons. We found that the estimated shadowing variance can be significantly overestimated if the two effects are not properly distinguished. In other words, to obtain proper shadowing variances, measurement (or ray tracing) data *have* to be analyzed on a street-by-street basis.

The paper furthermore presents a spatially consistent street-by-street (SbS) PL model for 28 GHz channels in urban micro cell (UMi) environment. The model parametrization example is based on a large PL dataset from ray-tracing simulations in NYC and in total includes 11 different BS locations.

The PL parameters are analyzed for a total of 28 LOS and 164 NLOS streets. The new PL and shadowing models provide a different PL slope, offset, shadow fading variance, and correlation distance for each street canyon, and can, therefore, provide a spatially consistent model that takes into account the observed non-stationarity of the PL behavior. Large variance is observed for all parameters. After careful analysis of the cross-correlations of the PL parameters and geometrical parameters, the NLOS streets are divided into three classes based on the street orientation compared to the BS. Finally, a simple simulation example on a street grid is shown and used to compare the proposed model to typical PL models, and the proposed SbS modeling principle is shown to be better in terms of spatial consistency.

REFERENCES

[1] A. F. Molisch, A. Karttunen, S. Hur, J. Park, and J. Zhang, "Spatially consistent pathloss modeling for millimeter-wave channels in urban environments," in *Proc. 10th Eur. Conf. Antennas Propag. (EuCAP)*, Apr. 2016, pp. 1–2.

[2] T. S. Rappaport *et al.*, "Millimeter wave mobile communications for 5G cellular: It will work!" *IEEE Access*, vol. 1, pp. 335–349, May 2013.

[3] J. G. Andrews *et al.*, "What will 5G be?" *IEEE J. Sel. Areas Commun.*, vol. 32, no. 6, pp. 1065–1082, Jun. 2014.

[4] T. S. Rappaport, J. N. Murdock, and F. Gutierrez, Jr., "State of the art in 60-GHz integrated circuits and systems for wireless communications," *Proc. IEEE*, vol. 99, no. 8, pp. 1390–1436, Aug. 2011.

[5] A. F. Molisch, *Wireless Communications*, 2nd ed. Hoboken, NJ, USA: Wiley, 2010.

[6] Accessed: Sep. 12, 2017. [Online]. Available: https://www.nist.gov/sites/default/files/documents/ctl/5G-Millimeter-Wave-Channel-Model-AllianceV2.pdf

[7] Accessed: Sep. 12, 2017. [Online]. Available: http://www.nist.gov/ctl/upload/5G-Millimeter-Wave-Channel-Model-AllianceV2.pdf

[8] *Study on Channel Model for Frequencies From 0.5 to 100 GHz*, document TR 38.901 V14.0.0, 3GPP, 2017.

[9] *5G Channel Model for Bands up to 100 GHz (v2.0)*, Aalto Univ., Espoo, Finland, Mar. 2016.

[10] P. Kyösti *et al.* (2008). *IST-4-027756 WINNER II, D1.1.2 V1.2, WINNER II Channel Models*. [Online]. Available: http://projects.celticinitiative.org/winner+/index.html

[11] A. Maltsev *et al.*, *Channel Models for 60 GHz WLAN Systems*, document IEEE 802.11-09/0334r7, 2010.

[12] T. S. Rappaport, G. R. Maccartney, M. K. Samimi, and S. Sun, "Wideband millimeter-wave propagation measurements and channel models for future wireless communication system design," *IEEE Trans. Commun.*, vol. 63, no. 9, pp. 3029–3056, Sep. 2015.

[13] M. K. Samimi, T. S. Rappaport, and G. R. MacCartney, Jr., "Probabilistic omnidirectional path loss models for millimeter-wave outdoor communications," *IEEE Wireless Commun. Lett.*, vol. 4, no. 4, pp. 357–360, Aug. 2015.

[14] S. Sun *et al.*, "Investigation of prediction accuracy and parameter stability of large-scale propagation path loss models for 5G wireless communications," *IEEE Trans. Veh. Technol.*, vol. 65, no. 5, pp. 2843–2860, Mar. 2016.

[15] W. Keusgen, R. J. Weiler, M. Peter, M. Wisotzki, and B. Gktepe, "Propagation measurements and simulations for millimeter-wave mobile access in a busy urban environment," in *Proc. 39th Int. Conf. Infr., Millim., Terahertz Waves (IRMMW-THz)*, Sep. 2014, pp. 1–3.

[16] K. Haneda, N. Omaki, T. Imai, L. Raschkowski, M. Peter, and A. Roivainen, "Frequency-agile pathloss models for urban street canyons," *IEEE Trans. Antennas Propag.*, vol. 64, no. 5, pp. 1941–1951, May 2016.

[17] X. Zhao *et al.*, "Comparisons of channel parameters and models for urban microcells at 2 GHz and 5 GHz [wireless corner]," *IEEE Antennas Propag. Mag.*, vol. 56, no. 6, pp. 260–276, Dec. 2014.

[18] M. K. Samimi and T. S. Rappaport, "3-D millimeter-wave statistical channel model for 5G wireless system design," *IEEE Trans. Microw. Theory Techn.*, vol. 64, no. 7, pp. 2207–2225, Jul. 2016.

[19] S. Hur *et al.*, "Proposal on millimeter-wave channel modeling for 5G cellular system," *IEEE J. Sel. Topics Signal Process.*, vol. 10, no. 3, pp. 454–469, Apr. 2016.

[20] S. Baek, Y. Chang, S. Hur, J. Hwang, and B. Kim, "3-dimensional large-scale channel model for urban environments in mmWave frequency," in *IEEE Int. Conf. Commun. Workshop (ICCW)*, Jun. 2015, pp. 1220–1225.

[21] Y. Chang, S. Baek, S. Hur, Y. Mok, and Y. Lee, "A novel dual-slope mm-wave channel model based on 3D ray-tracing in urban environments," in *Proc. IEEE 25th Annu. Int. Symp. Pers., Indoor, Mobile Radio Commun. (PIMRC)*, Sep. 2014, pp. 222–226.

[22] V. Erceg *et al.*, "An empirically based path loss model for wireless channels in suburban environments," *IEEE J. Sel. Areas Commun.*, vol. 17, no. 7, pp. 1205–1211, Jul. 1999.

[23] S. S. Ghassemzadeh, R. Jana, C. W. Rice, W. Turin, and V. Tarokh, "Measurement and modeling of an ultra-wide bandwidth indoor channel," *IEEE Trans. Commun.*, vol. 52, no. 10, pp. 1786–1796, Oct. 2004.

[24] Z. Li, R. Wang, and A. F. Molisch, "Shadowing in urban environments with microcellular or peer-to-peer links," in *Proc. 6th Eur. Conf. Antennas Propag. (EUCAP)*, Mar. 2012, pp. 44–48.

[25] W. M. Smith, "Urban propagation modeling for wireless systems," Ph.D. dissertation, Dept. Electr. Eng., Stanford Univ., Stanford, CA, USA, 2004.

[26] V. Erceg, S. Ghassemzadeh, M. Taylor, D. Li, and D. L. Schilling, "Urban/suburban out-of-sight propagation modeling," *IEEE Commun. Mag.*, vol. 30, no. 6, pp. 56–61, Jun. 1992.

[27] T. Abbas, A. Thiel, T. Zemen, C. F. Mecklenbruker, and F. Tufvesson, "Validation of a non-line-of-sight path-loss model for V2V communications at street intersections," in *Proc. 13th Int. Conf. Telecommun. (ITST)*, Nov. 2013, pp. 198–203.

[28] G. C. Hess and S. S. Gilbert, "Shadowing variability in an urban land mobile environment at 900 MHz," *Electron. Lett.*, vol. 26, no. 10, pp. 646–648, May 1990.

[29] S. Szyszkowicz, H. Yanikomeroglu, and J. Thompson, "On the feasibility of wireless shadowing correlation models," *IEEE Trans. Veh. Technol.*, vol. 59, no. 9, pp. 4222–4236, Nov. 2010.

[30] C. Gustafson, T. Abbas, D. Bolin, and F. Tufvesson, "Statistical modeling and estimation of censored pathloss data," *IEEE Wireless Commun. Lett.*, vol. 4, no. 5, pp. 569–572, Oct. 2015.

[31] A. Karttunen, A. F. Molisch, A. Wang, S. Hur, J. Zhang, and J. Park, "Distance dependence of path loss models with weighted fitting," in *Proc. IEEE Int. Conf. Commun. (ICC)*, May 2016, pp. 1–6.

[32] A. I. Sulyman, A. T. Nassar, M. K. Samimi, G. R. MacCartney, Jr., T. S. Rappaport, and A. Alsanie, "Radio propagation path loss models for 5G cellular networks in the 28 GHz and 38 GHz millimeter-wave bands," *IEEE Commun. Mag.*, vol. 52, no. 9, pp. 78–86, Sep. 2014.

[33] K.-W. Kim and S.-J. Oh, "Geometric optics-based propagation prediction model in urban street canyon environments," *IEEE Antennas Wireless Propag. Lett.*, vol. 15, pp. 1128–1131, Oct. 2016.

[34] J.-E. Berg, "A recursive method for street microcell path loss calculations," in *Proc. 6th Int. Symp. Pers., Indoor Mobile Radio Commun.*, vol. 1. Sep. 1995, pp. 140–143.

[35] M. Series, "Guidelines for evaluation of radio interface technologies for IMT-Advanced," ITU, Tech. Rep. ITU-R M.2135-1, Dec. 2009.

[36] P. Series, "Propagation data and prediction methods for the planning of short-range outdoor radiocommunication systems and radio local area networks in the frequency range 300 MHz to 100 GHz," ITU, Tech. Rep. ITU-R P.1411-8, Jul. 2015.

[37] Y. Wang, K. Venugopal, A. F. Molisch, and R. W. Heath, Jr., "Analysis of urban millimeter wave microcellular networks," in *Proc. IEEE 84th Veh. Technol. Conf. (VTC-Fall)*, Sep. 2016, pp. 1–5.

[38] *Wireless Insight: Wireless EM Propagation Software*, REMCOM, New York, NY, USA, 2015.

[39] K. R. Schaubach, N. J. Davis, and T. S. Rappaport, "A ray tracing method for predicting path loss and delay spread in microcellular environments," in *Proc. IEEE 42nd Veh. Technol. Conf.*, May 1992, pp. 932–935.

[40] L. Correia and P. Frances, "Estimation of materials characteristics from power measurements at 60 GHz," in *Proc. 5th IEEE Int. Symp. Pers., Indoor Mobile Radio Commun., Wireless Netw.-Catching Mobile Future*, Sep. 1994, pp. 510–513.

Aki Karttunen (M'13) received the M.Sc. (Tech.), Lic.Tech. (Tech.), and D.Sc. (Tech.) degrees from Aalto University, Espoo, Finland, in 2006, 2009, and 2013, respectively, all in electrical engineering. From 2013 to 2015, he was with the Department of Radio Science and Engineering, Aalto University. From 2015 to 2016, he was with the Department of Electrical Engineering, University of Southern California, Los Angeles, CA, USA. He is currently with the Department of Electronics and Nanoengineering, Aalto University. His current research interests include millimeter-wave channel measurements, prediction, and modeling.

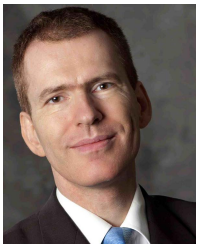

Andreas F. Molisch (S'88–M'95–SM'00–F'05) received the Dipl.-Ing., Ph.D., and Habilitation degrees from the Technical University of Vienna, Vienna, Austria, in 1990, 1994, and 1999, respectively. He subsequently was with AT&T (Bell) Labs Research, USA, Lund University, Lund, Sweden, and Mitsubishi Electric Research Laboratories, USA. He is currently a Professor and the Solomon-Golomb Andrewand-Erna-Viterbi Chair with the University of Southern California, Los Angeles. His current research interests are the measurement and modeling of mobile radio channels, multi-antenna systems, ultra-wideband communications and localization, novel modulation and multiple access systems, and wireless video distribution. He has authored, coauthored, or edited four books, among them the textbook *Wireless Communications*, (Wiley–IEEE Press), 19 book chapters, over 200 journal papers, 300 conference papers, over 80 patents, and 70 standards contributions. He has been an editor of a number of journals and special issues, the general chair, the technical program committee chair, or the symposium chair of multiple international conferences, and the chairman of various international standardization groups. He is a Fellow of the National Academy of Inventors, a Fellow of the AAAS, a Fellow of the IET, an IEEE Distinguished Lecturer, and a member of the Austrian Academy of Sciences. He has received numerous awards, among them the Donald Fink Prize of the IEEE and the Eric Sumner Award of the IEEE.

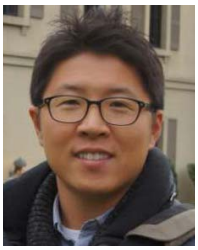

Sooyoung Hur (S'05–M'13) received the B.S degree in electrical engineering from Sogang University, Seoul, South Korea, in 2005, the M.S. degree in electrical engineering from the Korea Advanced Institute of Science and Technology, Daejeon, South Korea, in 2007, and the Ph.D. degree in electrical and computer engineering from Purdue University, West Lafayette, IN, USA, in 2013. Since 2013, he has been with the Communication Research Team, Samsung Electronics. His current research interests are in physical layer communications and in particular channel measurements, cellular and mm-wave communications, and signal processing for wireless communications, especially 5G communication technologies.

Jeongho Park received the B.S., M.S., and Ph.D. degrees from Yonsei University in 1997, 2000, and 2005, respectively, all in electronic engineering. Since 2005, he has been with Samsung Electronics, where he was involved in research and development of wireless communications. He is currently the Director of the Next Generation Communications Business Team, Samsung Electronics, and leads the research and development of break-through technologies in 5G and beyond 5G area. Standardization is also his interest including the IEEE 802, 3GPP RAN, and ITU-R IMT-Systems.

Charlie Jianzhong Zhang (S'00–M'03–SM'09–F'16) received the Ph.D. degree from the University of Wisconsin, Madison WI, USA. He was with the Nokia Research Center from 2001 to 2006, where he was involved in the IEEE 802.16e (WiMAX) standard and EDGE/CDMA receivers, and from 2006 to 2007, he was with Motorola, where he was involved in 3GPP HSPA standards. From 2009 to 2013, he served as the Vice Chairman of the 3GPP RAN1 group and led the development of LTE and LTE-Advanced technologies, such as 3-D channel modeling, UL-MIMO and CoMP, and Carrier Aggregation for TD-LTE. He is currently the Vice President and the Head of the Standards and Mobility Innovation Laboratory, Samsung Research America, where he leads research, prototyping, and standards for 5G cellular systems and future multimedia networks.